A Resonant Tunneling Quantum-Dot Infrared Photodetector

Xiaohua Su, Subhananda Chakrabarti, Pallab Bhattacharya, *Fellow, IEEE*, Gamini Ariyawansa, and A. G. Unil Perera, *Senior Member, IEEE*

***Abstract*—A novel device—resonant tunneling quantum-dot infrared photodetector—has been investigated theoretically and experimentally. In this device, the transport of dark current and photocurrent are separated by the incorporation of a double barrier resonant tunnel heterostructure with each quantum-dot layer of the device. The devices with $In_{0.4}Ga_{0.6}As$–GaAs quantum dots are grown by molecular beam epitaxy. We have characterized devices designed for $\sim 6\ \mu$m response, and the devices also exhibit a strong photoresponse peak at $\sim 17\ \mu$m at 300 K due to transitions from the dot excited states. The dark currents in the tunnel devices are almost two orders of magnitude smaller than those in conventional devices. Measured values of $J_{\rm dark}$ are 1.6×10^{-8} A/cm^2 at 80 K and 1.55 A/cm^2 at 300 K for 1-V applied bias. Measured values of peak responsivity and specific detectivity D^* are 0.063 A/W and 2.4×10^{10} cm $\cdot$ Hz$^{1/2}$/W, respectively, under a bias of 2 V, at 80 K for the 6-μm response. For the 17-μm response, the measured values of peak responsivity and detectivity at 300 K are 0.032 A/W and 8.6×10^{6} cm $\cdot$ Hz$^{1/2}$/W under 1 V bias.**

***Index Terms*—Infrared detectors, quantum dots, responsivity, specific detectivity.**

I. Introduction

THE DETECTION of long wavelength radiation remains a difficult challenge to semiconductor technology. Especially difficult is being able to detect weak signals at high temperatures since thermal effects create an exponentially increasing dark (noise) current. The quantum-dot infrared photodetector (QDIP), with self-organized quantum dots in the active region, is positioned to become an important technology in the field of infrared (IR) detection [1]–[8]. The three-dimensional carrier confinement and favorable dynamics of hot carriers in the quantum dots promises normal-incidence operation, low dark current, and high operating temperatures. As in the quantum-well infrared photodetector (QWIP), absorption of IR light leads to an intersubband (or intersublevel) transition of carriers, which are eventually collected by the contacts to contribute to the photocurrent. For large photocurrent and responsivity, a large carrier lifetime $\tau_{\rm eff}$, which is the time elapsed before photoexcited carrier falls back into ground state of any quantum dot, is essential. Previous studies undertaken by us have shown that $\tau_{\rm eff}$, which is bias-dependent, varies in the range of 30 to 100 ps [9].

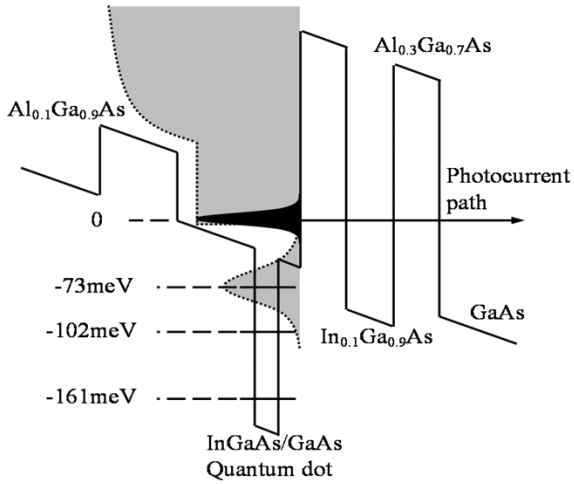

Fig. 1. Schematic diagram of the conduction band profile of an InAs–GaAs tunneling QDIP (T-QDIP) with a GaAs–$Al_{0.3}Ga_{0.7}As$ resonant tunneling heterostructure under an applied bias. Also shown schematically are the electron density of states (shaded region) and the energy distribution of the tunneling photoexcited electrons (shaded black). The calculated energy levels in the well and dot (see text) are indicated.

A critical parameter in the operation of IR detectors is the dark current, which should be as small as possible to enhance the detectivity D^*. In the commonly investigated vertical QDIPs, with or without confined dot layers [dot-in-a-well (DWELL) structure], the dark current is determined by thermionic emission and field-assisted tunneling [10]. The dark current can be effectively reduced by increasing the dot confinement potential, by increasing the thickness of the active region, or by incorporating additional energy barriers. Unfortunately, these measures also reduce the photocurrent, since the transport paths of the carriers are identical. It is therefore essential to explore device designs by which the dark current can be decoupled from the thermal background which enhances thermionic emission at high operating temperatures, but the device photocurrent is not affected.

In the present study, we have investigated, theoretically and experimentally, the properties of a novel QDIP design in which a resonant tunneling heterostructure is incorporated with each quantum dot layer. The conduction band diagram of a single period of the active region is schematically shown in Fig. 1. The resonant tunneling double barrier is so designed that the electron tunneling probability is unity at an energy coincident with the peak detection wavelength. The tunneling probability will be significantly smaller at energies which are removed from this

Manuscript received December 22, 2004; revised March 14, 2005. The work performed at the University of Michigan was supported in part by the Army Research Office MURI program under Grant DAAD19-01-1-0462 and at the work performed at Georgia State University was supported in part by the National Science Foundation under Grant ECS-0140434.

X. H. Su, S. Chakrabarti, and P. Bhattacharya are with the Solid State Electronics Laboratory, Department of Electrical Engineering and Computer Science, University of Michigan, Ann Arbor, MI 48109-2122 USA (e-mail: pkb@eecs.umich.edu).

G. Ariyawansa and A. G. U. Perera are with the Department of Physics and Astronomy, Georgia State University, Atlanta, GA 30303 USA.

Digital Object Identifier 10.1109/JQE.2005.848901

optimum value. Thus the transport of the carriers contributing to the dark current, which have a broad energy distribution at high temperatures, will be inhibited and the dark current will be reduced. A single $Al_{0.1}Ga_{0.9}As$ barrier is also included on the side of the dot opposite to the tunnel barriers. The inclusion of this layer creates a quantum well and quasi-bound final states for the photoexcited electrons from the quantum dots. These states are designed to resonate with the tunnel states in the double barrier heterostructure. Furthermore, the energy position of the states in the well can be tuned by varying the distance of the AlGaAs barrier from the quantum dot layer, thereby providing tunability of the absorption peak wavelength.

In what follows, the calculation of dark current in a QDIP and its reduction with the resonant tunneling barriers is described in Section II. The molecular beam epitaxial (MBE) growth and fabrication of the devices and a description of the measurements are outlined in Section III. The results are described and discussed in Section IV. Finally, a summary is provided in Section V.

II. Calculation of Dark Currents

The dark current in a QDIP, as a function of applied bias V, is given by

$$I_D(V) = ev(V)n_{em}(V)A \tag{1}$$

where v is the average electron drift velocity in the barrier material, n_{em} is the concentration of electrons excited out of the quantum dots by thermionic emission and tunneling, and A is the detector area. Here

$$v(V) = \frac{\mu F(V)}{\sqrt{1 + \left(\frac{\mu F(V)}{v_s}\right)^2}} \tag{2}$$

$$n_{em}(V) = \int_{-\infty}^{\infty} N(E)f(E)T(E,V)dE \tag{3}$$

where μ is the electron mobility, F is the bias-dependent electric field, v_s is the electron saturation velocity, $f(E)$ is the Fermi–Dirac distribution function, $N(E)$ is the density of states, and $T(E,V)$ is the tunneling probability across a triangular barrier. Here E is the total energy, rather than the energy associated with the tunneling direction, since in a real system electron scattering causes the electron wave function to decay in the barriers in accordance with the total energy of the electrons. The tunneling probability is calculated using the transfer matrix method. For both square and triangular potential barriers, segmentation is employed to simplify the calculations, wherein the barrier potential is a constant V_j in the jth segment. The corresponding one-dimensional plane wave associated with the electron is

$$\psi_j(z) = A_j \exp(ik_j z) + B_j \exp(-ik_j z) \tag{4}$$

where $k_j = 2\pi\sqrt{2m_j^*(E - V_j)}/h$, h is Planck's constant and m_j^* is the effective mass. The tunneling probability is then given by

$$T(E) = \frac{m_{N+1}^* k_0}{(m_0^* k_{N+1} M_{22}^2)} \tag{5}$$

TABLE I
Physical Parameters Used in the Calculation of Dark Current Density in Conventional and T-QDIPs

Parameters	Values
Surface Density of dots	5×10^{10} cm^{-2}
Inhomogeneous broadening	40 meV
Wetting layer thickness	3 monolayer
AlAs/GaAs band offset	60%
GaAs/InAs Band offset	60%
Electron mobility	1000 cm^{2}V^{-1}s^{-1}
Electron saturation velocity	1×10^7 cm/s
QD electron Fermi level	0.145 eV below GaAs conduction band edge

where M_{22} is the element of the transfer matrix $\prod_{n=1}^{N+1} M_n$ with both column and row index equal to 2. The subscripts 0 and $N+1$ correspond to points outside the barriers. The density of states $N(E)$ is given by

$$N(E) = \sum_i \frac{2N_d}{L_p}\frac{1}{\sqrt{2\pi}\sigma}\exp\left(\frac{(E-E_i)^2}{2\sigma^2}\right) + \frac{4\pi m^*}{L_p h^2}H(E - E_W) + \frac{8\pi\sqrt{2}}{h^3}m^{*(3/2)}\sqrt{E - E_C}H(E - E_C) \tag{6}$$

where in the first term, N_d is the surface density of the dots, and E_i is the energy of the discrete dot levels. The values of E_i are determined from an eight-band $\mathbf{k}\cdot\mathbf{p}$ calculation, assuming a pyramidal shape of the dots and accounting for built-in strain through the valence force field model [8]. A Gaussian distribution accounts for the inhomogeneous broadening due to size inhomogeneity of the dots. The second term is the density of the wetting layer states, which is calculated by assuming a two-dimensional electron gas in the wetting layer. E_w is the energy of the wetting layer state and since the thickness of the wetting layer is small (less than two monolayers), only one confined state exists in this layer. The function $H(x) = 1$ for $x \geq 0$ and $H(x) = 0$ for $x < 0$. The last term gives the density of states in the bulk barrier material and E_c is the energy of the conduction band edge therein.

Equations (1)–(6) are used to calculate the dark current in a conventional QDIP without tunnel barriers. Some of the important material parameters are listed in Table I. The same equations can also be used to calculated the dark currents in a tunneling QDIP (T-QDIP) after suitable modification of the density of states $N(E)$ and the tunneling probability $T(E,V)$ for the double barrier resonant tunneling heterostructure. In performing the calculations and the growth and characterization of the two types of heterostructures, it is ensured that the total thickness of each dot period is the same for both devices (QDIP and T-QDIP), such that the electric field in the active region with the same applied bias is nearly identical.

III. Epitaxial Growth and Device Fabrication

As described in Section II, the bound state energies in the quantum dots, as indicated in Fig. 1, were calculated by an eight-

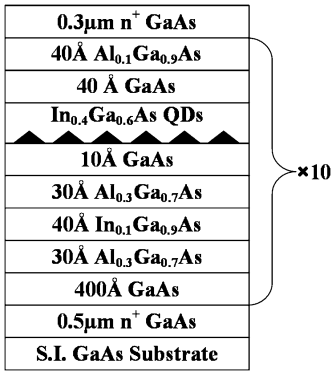

Fig. 2. Schematic heterostructure of a tunnel-QDIP grown by molecular beam epitaxy. All the other layers, except the Si-doped GaAs contact layers, are undoped.

band $\mathbf{k}\cdot\mathbf{p}$ model [11]. The energy levels in the quantum well, taking into account the presence of the two-dimensional wetting layer that precedes the three-dimensional island in every dot layer, is calculated by solving the one-dimensional Schrödinger equation. The calculated value of the absorption coefficient in an $In_{0.4}Ga_{0.6}As$ quantum dot is $\sim 10^4$ cm^{-1} for normal incidence [12]. While this value seems quite large, it should be noted that the absorbing region of a quantum dot layer is very thin ($\sim$100 Å). Therefore multiple dot layers are required to absorb a significant fraction of the incoming IR light.

The tunneling QDIP heterostructures were grown by molecular beam epitaxy in an EPI Mod Gen II system equipped with an arsenic cracker. The device heterostructure, grown on (001)-oriented semi-insulating GaAs substrate, is schematically shown in Fig. 2. The GaAs and $Al_{0.3}Ga_{0.7}As$ layers were grown at 610 °C and the quantum dots were grown at 500 °C. Before initiating the growth of the quantum dots, 10 Å of GaAs was grown on the $Al_{0.3}Ga_{0.7}As$ barrier of the resonant tunneling heterostructure, to smoothen the growing surface. This was followed by the deposition of 6 monolayers of InGaAs to form the self-organized quantum dots. The dot layer is undoped and *in situ* reflection high energy electron diffraction (RHEED) in the growth temperature was used to monitor the formation of the quantum dots and, in particular, observe the transition from the two-dimensional wetting layer (after four monolayers) to three dimensional islands. A $Al_{0.1}Ga_{0.9}As$ barrier of thickness 40 Å is incorporated on the other side of the dot, opposite to the double barrier. As shown in Fig. 2, ten dot layers with accompanying double barrier structures were grown, separated by 400-Å GaAs barrier layers. Growth is terminated with a 0.2-μm silicon-doped ($n = 2 \times 10^{18}$ cm^{-3}) GaAs top contact layer.

A standard, three-step photolithography, wet-etching and contact metallization process was employed to fabricate the vertical n-i-n mesa-shaped QDIPs. The first step is the deposition of Ni–Ge–Au–Ti–Au by electron beam evaporation to form the top ring contact, defined by photolithography and lift-off techniques. Next, wet etching is done, with the top contact as the mask, to define the mesa-shaped active region for a single pixel. The same multilayered metal evaporation is next done to define the bottom ring contact. The active area of the detector exposed to IR radiation is determined by the inner radius of the top ring contact (200 μm) and is approximately 1.26×10^5 μm^2.

IV. Results and Discussion

A. Measurement Techniques

The devices are mounted on chip carriers with silver epoxy and individual devices are wire bonded to separate leads of the carriers. These are then mounted in a variable temperature liquid He cryostat. The dark current–voltage $(I$–$V)$ characteristics are measured with a Hewlett-Packard 4145 Semiconductor Parameter Analyzer. Measurements are made for both bias polarities, where a positive bias denotes a positive polarity of the top contact. Therefore, the band diagram of Fig. 1(a) is for a negative bias.

The spectral response and calibrated responsivity spectra of the devices are measured, under normal incidence, with a globar broad-band source. The spectral response of the device under test and a composite bolometer, with a known sensitivity, are measured with a S2000 Fourier transform infrared spectrometer (FTIR). The two spectra are obtained concurrently with the same combination of optical window, beamsplitter and filters, so that the optical path is identical. The device spectrum (I_d) is then divided by the bolometer spectrum (I_b) and multiplied by the bolometer sensitivity (S_0) to obtain the voltage responsivity of the device

$$R\left(\frac{V}{W}\right) = \frac{GI_dS_0}{I_b}. \tag{7}$$

Here G is a geometrical factor which corrects for differences in the radiation-incident-area of the detector and the bolometer. To obtain the current responsivity, the voltage responsivity is divided by the effective resistance. As the detector and the load resistor act as a voltage divider the effective resistance R_e is the parallel resistance of the load R_l and the detector dynamic resistance $R_d(= dV/dI)$, yielding $R_e = R_lR_d/(R_l+R_d)$. The final current responsivity is given by

$$R\left(\frac{A}{W}\right) = \frac{GI_dS_0(R_l+R_d)}{(R_lR_dI_b)}. \tag{8}$$

The specific detectivity (D^*) of the devices at different temperatures and applied biases is obtained from the measured peak responsivity R_p and noise density spectra, S_i. The latter are measured with a dual channel fast Fourier transform (FFT) signal analyzer and a low noise pre-amplifier. A thick copper plate is used as the radiation block to provide the dark conditions for the measurements. The value of D^* is calculated from

$$D^* = \frac{R_pA^{1/2}}{S_i^{1/2}} \left[\frac{\text{cm}\cdot\text{Hz}^{1/2}}{\text{W}^{-1}}\right] \tag{9}$$

where A is the illuminated area of the detector.

B. Dark Current and Spectral Response

Measured bias-dependent dark current densities, in the temperature range of 80–300 K are shown in Fig. 3(a). A slight asymmetry observed for opposite bias polarities in the low-temperature data arises from the asymmetry in the dot heterostructure. In Fig. 3(b) measured dark current data at 140 K are compared with calculated values for both conventional and tunnel QDIPs. Similar data have been reported by us previously [13],

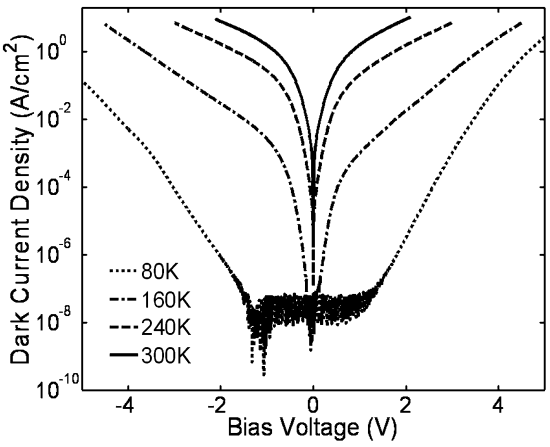

(a)

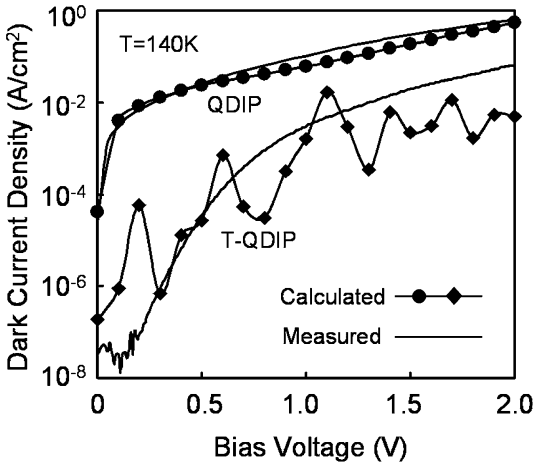

(b)

Fig. 3. (a) Measured dark current density as a function of bias in the temperature range 80–300 K. (b) Comparison of calculated and measured dark current densities as a function of bias voltage at $T = 140$ K for conventional and T-QDIPs using $In_{0.4}Ga_{0.6}As$–GaAs quantum dots.

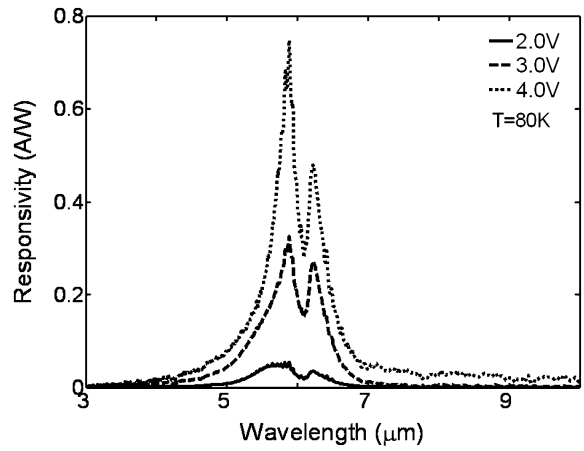

(a)

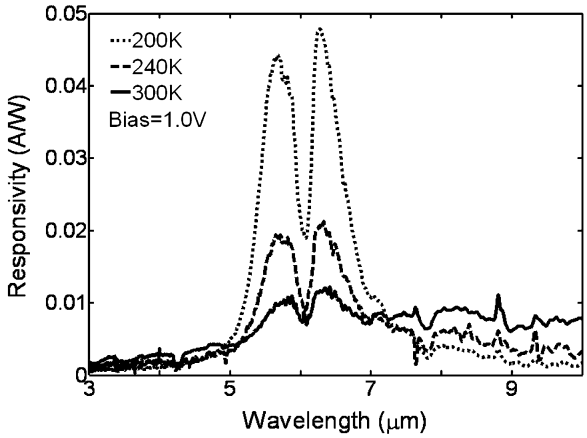

(b)

Fig. 4. Measured spectral responsivity of T-QDIP (a) in the bias range 2–4 V at 80 K and (b) in the temperature range 240–300 K under 2-V bias.

but are included here for completeness. It is evident that there is good agreement between calculated and measured dark currents and there is a significant reduction in dark currents with the incorporation of the resonant tunnel filters. The oscillations in the calculated bias-dependent dark current of the T-QDIP reflect multiple tunneling resonances across all the QD layers in the active region. These resonances are not observed in the measured data for two reasons: the multiple states smooth the current and the diodes are quite large (400-μm diameter). The disagreement at large bias values is because of nonequilibrium conditions which were neglected in our calculation. From the data of Fig. 3(a), the values of $J_{\rm dark}$ at a bias of 1 V are 1.61×10^{-8}, 0.12, and 1.55 A/cm^2 at 80, 200, and 300 K, respectively. These are the lowest dark currents measured in QDIPs or any other semiconductor-based IR detectors.

Fig. 4(a) depicts the dominant mid-IR spectral response of the tunnel QDIP for different bias values measured at 80 K. Fig. 4(b) shows the same peaks measured at high temperatures, up to 300 K. Several features in these figures are worth noting. On closer examination, it is apparent that the response centered at 6 μm consists of two closely spaced peaks at 5.7 and 6.2 μm. The transition wavelength of 6 μm is in excellent agreement with the designed and calculated transition energy of 161 meV for the photoexcited electrons from the ground state in the quantum dot to the quasi-bound state in the well. The peaks at 5.7 and 6.2 μm arise from overlap of the wavefunctions of the quantum well states and the bound states of the double barrier heterostructure. The twin peaks provide experimental evidence of resonant tunneling in the operation of the device. The estimated value of $\Delta\lambda/\lambda$ for the 5.7-μm peak is 6%. From the data of Fig. 4(a) and (b), the peak responsivity and quantum efficiency are, respectively, 0.75 A/W and 16% (4-V bias) at 80 K and 0.05 A/W and 1.1% (2-V bias) at 300 K.

Under no illumination, the dark current flowing through the device is due to generation-recombination processes resulting from carrier trapping into and thermionic emission from the quantum dots. Under illumination, photoemission from the quantum dots contributes to an additional current component, the photocurrent, and an additional trapping into the quantum dots. Some of the electrons falling into the quantum-dot well can kick carriers into emission at low bias values, adding to the photocurrent, and thereby generating gain. This is an avalanche gain mechanism which occurs at biases lower than those in conventional junction photodiodes. In addition, QDIPs can display photoconductive gain. The physical mechanism responsible for photoconductive gain in QDIPs is the maintenance of charge neutrality in the dot active region of the device. When electrons are photoexcited from the dots to the continuum states, they drift toward the contact layer. The electrons may either be

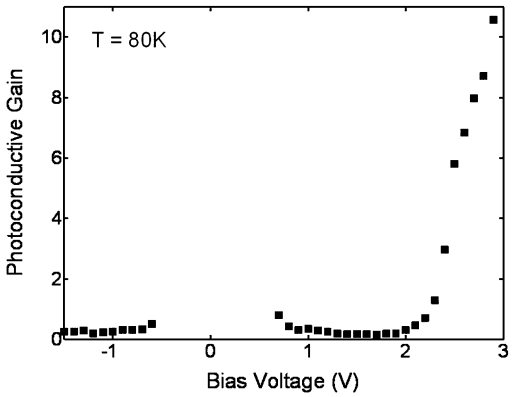

Fig. 5. Measured gain of 5.7-μm response peak as a function of bias at 80 K.

captured by successive dots in transit or may reach the contact. In the latter case, an electron is injected from the opposite contact and the process will continue until the electron is lost by capture into the dots.

Experimentally, photoconductive g is obtained from the relation [14]

$$g = \frac{S_i}{4qI_{\rm dark}} + \frac{1}{2N} \tag{10}$$

where $I_{\rm dark}$ is the measured dark current and N is the number of quantum-dot layers. Direct measurement of the noise current and the dark current provides a measure of the device gain. The measured gain of the T-QDIP is plotted in Fig. 5 as a function of bias. In the operating bias range of interest, 1–2 V, the gain is unity. The increase in gain beyond 2 V is believed to be due to the onset of avalanche process described above. Therefore, the responsivity values discussed above reflect the true absorption and photoresponse of the devices. This is the first report of room temperature photoresponse in the mid-IR range from any QDIP.

While the 6-μm response is dominant for ambient temperatures below 200 K, long wavelength IR (LWIR) response at 11 and 17 μm are observed in the T-QDIPs at higher temperatures. The 17-μm response peak increases with temperature and at 300 K its peak responsivity is higher than that of the 6-μm peak. These transition wavelengths are in excellent agreement with the energy separation of the dot first and second excited states and the quasi-bound well states (102 and 73 meV), which suggests that the dot excited states gets filled as the temperature is raised. The LWIR response at high temperatures is depicted in Fig. 6. It may be noted that a peak responsivity of 0.16 A/W is measured at room temperature for the 17-μm response.

C. Specific Detectivity

The measured values of D^* at $T = 80$ K are plotted in Fig. 7 as a function of bias. The value of D^* reaches a maximum value of 2.4×10^{10} cm $\cdot$ Hz$^{1/2}$/W at 2 V and decreases again due to the monotonic increase of the dark current with bias. While this value is amongst the highest measured for QDIPs at 80 K, it is clear that further optimization of the device heterostructure is needed to increase the values of both R_p and D^* by at least an order of magnitude. Interestingly, the measured value of D^* for the 17-μm transition at 300 K is $\sim 10^7$ cm $\cdot$ Hz$^{1/2}$/W, which is probably the highest value obtained for a semiconductor-based IR detector at that temperature.

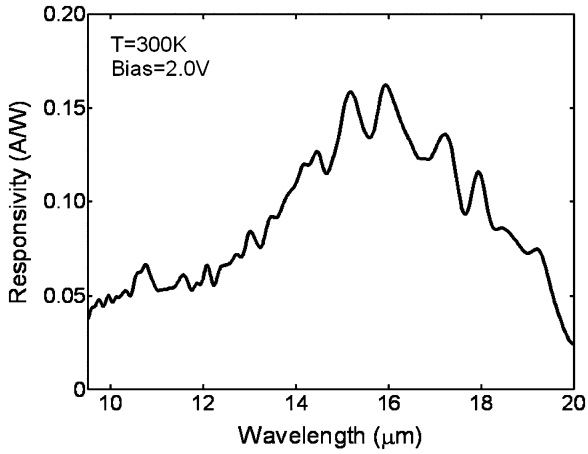

Fig. 6. Measured spectral responsivity in the long wavelength range at 300 K under a bias of 2 V.

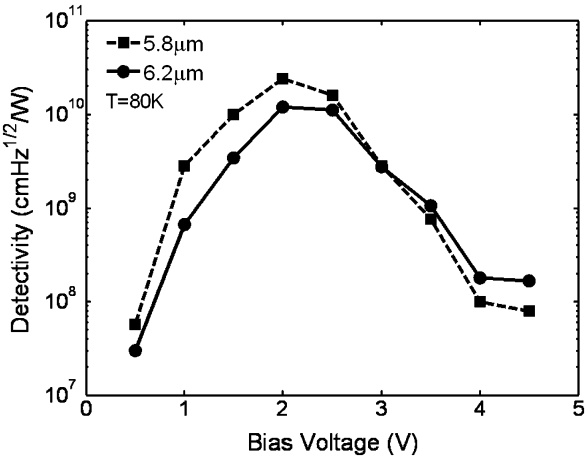

Fig. 7. Peak detectivity as a function of bias for the 5.7- and 6.2-μm response at 80 K derived from noise spectra measurements.

V. Summary

In conclusion, we describe the properties of a novel QDIP in which a resonant tunneling filter is incorporated with each quantum dot layer in the active region of the device. In this tunnel QDIP (T-QDIP) the double barrier resonant tunneling heterostructure selectively transmits the photoexcited carriers, which contribute to the photocurrent and responsivity, while blocking the carriers, with a broad energy distribution, which contribute to the dark current. The calculation of the dark currents is described and the calculated dark current agrees well with the measured values. A reduction in the dark current, by almost two orders of magnitude, is observed. In accordance with the design, a dominant responsivity peak at ~ 6 μm is observed. The peak responsivity is 0.75 A/W at 80 K for a bias of 4 V and the specific detectivity D^* is 2.4×10^{10} cm $\cdot$ Hz$^{1/2}$/W at the same temperature and an applied bias of 2 V. The devices also exhibit a long wavelength response at 17 μm at room temperature, with reasonable values of peak responsivity and detectivity.

References

[1] J. Phillips, K. Kamath, and P. Bhattacharya, "Far-infrared photoconductivity in self-organized InAs quantum dots," *Appl. Phys. Lett.*, vol. 72, pp. 2020–2021, 1998.

[2] D. Pan, E. Towe, and S. Kennerly, "Normal incidence intersubband (In,Ga)As/GaAs quantum dot infrared photodetectors," *Appl. Phys. Lett.*, vol. 73, pp. 1937–1939, 1998.
[3] S. Maimon, E. Finkman, G. Bahir, S. E. Schacham, J. M. Garcia, and P. M. Petroff, "Intersublevel transitions in InAs/GaAs quantum dot photodetectors," *Appl. Phys. Lett.*, vol. 73, pp. 2003–2005, 1998.
[4] J. Phillips, P. Bhattacharya, S. W. Kennerly, D. W. Beekman, and M. Dutta, "Self-assembled InAs-GaAs quantum-dot intersubband detectors," *IEEE J. Quantum Electron.*, vol. 35, no. 6, pp. 936–943, Jun. 1999.
[5] E. T. Kim, A. Madhukar, Z. Ye, and J. C. Campbell, "High detectivity InAs quantum dot infrared photodetector," *Appl. Phys. Lett.*, vol. 84, pp. 3277–3279, 2004.
[6] S. Chakrabarti, A. D. Stiff-Roberts, P. Bhattacharya, S. D. Gunapala, S. Bandara, S. B. Rafol, and S. W. Kennerly, "High temperature operation of InAs-GaAs quantum dot infrared photodetectors with large responsivity and detectivity," *IEEE Photon. Technol. Lett.*, vol. 16, no. 5, pp. 1361–1363, May 2004.
[7] S. Raghavan, P. Rotella, A. Stintz, B. Fuchs, S. Krishna, C. Morath, D. A. Cardimona, and S. W. Kennerly, "High-responsivity, normal-incidence long-wave infrared ($\lambda \sim 7.2\ \mu$m) InAs/$In_{0.15}Ga_{0.85}As$ dots-in-a-well detector," *Appl. Phys. Lett.*, vol. 81, pp. 1369–1372, 2002.
[8] S. Chakrabarti, A. D. Stiff-Roberts, P. Bhattacharya, and S. W. Kennerly, "High responsivity AlAs/InAs/GaAs superlattice quantum dot infrared detector," *Electron. Lett.*, vol. 40, pp. 197–198, 2004.
[9] J. Urayama, T. B. Norris, J. Singh, and P. Bhattacharya, "Observation of phonon bottleneck in electronic relaxation," *Phys. Rev. Lett.*, vol. 86, pp. 4930–4933, 2001.
[10] A. D. Stiff-Roberts, X. H. Su, S. Chakrabarti, and P. Bhattacharya, "Contribution of field-assisted tunneling emission to dark current in InAs–GaAs quantum dot infrared photodetectors," *IEEE Photon. Technol. Lett.*, vol. 16, no. 3, pp. 867–869, Mar. 2004.
[11] H. Jiang and J. Singh, "Strain distribution and electronic spectra of InAs/GaAs self-assembled dots: An eight-band study," *Phys. Rev. B.*, vol. 56, pp. 4696–4701, 1997.
[12] B. Kochmann, A. D. Stiff-Roberts, S. Chakrabarti, J. D. Phillips, S. Krishna, J. Singh, and P. Bhattacharya, "Absorption, carrier lifetime and gain in InAs–GaAs quantum dot infrared photodetectors," *IEEE J. Quantum Electron.*, vol. 39, no. 3, pp. 459–467, Mar. 2003.
[13] X. H. Su, S. Chakrabarti, A. D. Stiff-Roberts, J. Singh, and P. Bhattacharya, "Quantum dot infrared photodetector design based on double barrier resonant tunneling," *Electron. Lett.*, vol. 40, pp. 1082–1083, 2004.
[14] A. D. Stiff, S. Krishna, P. Bhattacharya, and S. W. Kennerly, "Normal-incidence, high-temperature, midinfrared, InAs-GaAs vertical quantum-dot infrared photodetector," *IEEE J. Quantum Electron.*, vol. 37, no. 11, pp. 1412–1419, Nov. 2001.

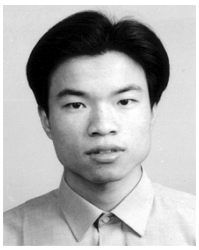

Xiaohua Su received the B.S. degree in material science from University of Science and Technology of China, Hefei, China, in 2000, and the M.S. degrees in physicsand electrical engineering from the Georgia Institute of Technology, Atlanta, in 2002 and 2003, respectively. He is currently working toward the Ph.D. degree in electrical engineering at the University of Michigan, Ann Arbor, where he is researching quantum-dot infrared photodetectors.

Subhananda Chakrabarti received the B.Sc. degree in physics from R. K. Mission Residential College (Narendrapur), Calcutta, India, and the M.Sc. and Ph.D. degrees from the Department of Electronic Science, University of Calcutta, India, in 1993 and 2000, respectively.

He was a Postdoctoral Fellow in the School of Engineering Science, Simon Fraser University, Burnaby, BC, Canada. He joined the Department of Electrical Engineering and Computer Science, University of Michigan, Ann Arbor, in May 2001 as a Research Fellow. His current research interests include molecular-beam-epitaxial growth of III–V semiconductors and quantum-dot infrared photodetectors.

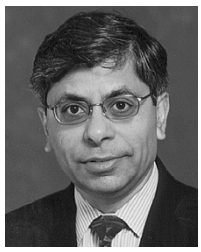

Pallab Bhattacharya (M'78–SM'83–F'89) received the Ph.D. degree from the University of Sheffield, Sheffield, U.K., in 1978.

He is currently the James R. Mellor Professor of Engineering and Professor of Electrical Engineering and Computer Science at The University of Michigan at Ann Arbor. His teaching and research interests include molecular beam epitaxy of elemental and III–V compound semiconductors, materials characterization, electronic and opto-electronic devices, and opto-electronic integrated circuits. From 1978 to 1983, he was with Oregon State University, Corvallis, and since then he has been with the University of Michigan at Ann Arbor. From 1981 to 1982, he was an Invited Professor at the Ecole Polytechnic Federale de Lausanne, Lausanne, Switzerland. He has authored or co-authored over 300 technical papers in archival journals. He authored the textbook *Semiconductor Optoelectronic Devices* (Englewood Cliffs, NJ: Prentice-Hall, 1994, 1st ed., and 1997, 2nd ed). He edited *Properties of Lattice-Matched and Strained InGaAs* (U.K.: INSPEC, 1993) and *Properties of III–V Quantum Wells and Superlattices* (U.K.: INSPEC, 1996).

Dr. Bhattacharya is a Fellow of the Optical Society of America and a member of the American Physical Society and Sigma Xi. He is an Editor of the IEEE TRANSACTIONS ON ELECTRON DEVICES. He has served on the Advisory Board of the Electrical and Communications Systems Division, National Science Foundation. He has also served on several other committees and panels in government, industry, and technical conferences. He was the recipient of the Parker Rhodes Scholarship presented by the University of Sheffield, the Research Excellence Award presented by the University of Michigan at Ann Arbor, the Alexander von Humboldt Award, the John Simon Guggenheim Fellowship, IEEE Lasers and Electro-Optics Society (LEOS) Distinguished Lecturer Award, the SPIE Technology Achievement Award, the IEEE Electron Devices Society Paul Rappaport Award, the IEEE LEOS Engineering Achievement Award, The University of Michigan Distinguished Faculty Achievement Award, and the S. S. Attwood Award presented by the University of Michigan at Ann Arbor.

Gamini Ariyawansa received the B.S. degree (first-class hons.) from the University of Peradeniya, Peradeniya, Sri Lanka, in 2001, the M.S. degree from Georgia State University, Atlanta, in 2005, where he is currently working on toward the Ph.D. degree.

His research interest is in infrared detectors. He has published four papers.

A. G. Unil Perera (SM'97) received the B.S. degree (first-class hons.) in physics from the University of Colombo, Sri Lanka, in 1981 and the M.S. and Ph.D. degrees from the University of Pittsburgh, Pittsburgh, PA, in 1983 and 1987, respectively.

Until 1992, he was a Research Assistant Professor at the University of Pittsburgh. In 1992, he joined Georgia State University, Atlanta, where he is currently a Full Professor. His research embraces development of semiconductor optroelectronic devices ranging from biology to electronics, as well as the search for fractional charge impurities (quarks) in semiconductors. He is the Director of the Interaction of Radiation with Matter Laboratory (IRML) and is a member of the Center for Neural Communication and Computation and also the Graduate Director of Physics. He has published five book chapters and more than 80 research articles and has a patent on infrared detectors.

Dr. Perera won the Outstanding Science Student of the Year Award at the University of Colombo, and was awarded the 1995 Junior Faculty Award, and the 1999 Faculty Achievement Award at Georgia State University. He is a member of APS and SPIE.